

CERAMIC MATERIALS FOR PRIMARY LOOP MAGNETIC FLOWMETERS AT NUCLEAR POWER PLANTS

Subtask 2.3 of

INTERNATIONAL NUCLEAR ENERGY RESEARCH INITIATIVE

Between
United States of America and Republic of Korea

Project 2002-020-K

*Development Of Enhanced Reactor Operation Strategy Through Improved
Sensing And Control At Nuclear Power Plants*

Stephen D. Nunn & David E. Holcomb—Oak Ridge National Laboratory
Chong Eun Chung & Byung Soo Moon—Korean Atomic Energy Research Institute
Don W. Miller & Joseph W. Talnagi—The Ohio State University

Final Project Report

February 2005

This Page Intentionally Left Blank

Table of Contents

1	<i>Project Summary</i>	1
2	<i>Background</i>	2
2.1	Project Rationale	2
2.2	Magnetic Flowmeter Overview	3
2.2.1	Commercial Experience Base	3
2.2.2	Physical Principals of Operation.....	3
2.2.3	Advanced Architectures	5
2.2.4	Operational Limitations	5
2.3	Competing Technologies	6
2.3.1	Venturi and Differential Pressure Based Flowmeter	6
2.3.2	Ultrasonic Flowmeters.....	6
3	<i>Experimental Approach</i>	8
4	<i>Results and Discussion</i>	11
4.1	Material, design, and process selection	11
4.2	Radiation exposure and property evaluation	15
4.3	Component assembly evaluation	20
5	<i>Conclusions</i>	21

Table of Figures

FIGURE 1—CONCEPTUAL ILLUSTRATION OF A MAGNETIC FLOWMETER WITH LARGE SIZE CAPACITIVELY COUPLED ELECTRODES.....	4
FIGURE 2—TRANSIT TIME ULTRASONIC FLOWMETER CONCEPTUAL ARRANGEMENT	7
FIGURE 3—CONCEPTUAL OPERATION OF CROSS-CORRELATION ULTRASONIC FLOWMETER	8
FIGURE 4— ILLUSTRATION OF THE LAYERED ALUMINA CERAMIC TEST SAMPLE WITH AN EMBEDDED PT ELECTRODE USED FOR RADIATION EXPOSURE TESTING AT KAERI AND OSURR.....	11
FIGURE 5— FLOWCHART SHOWING THE SEQUENCE OF OPERATIONS IN THE GELCASTING PROCESS.....	13
FIGURE 6—COMPARISON OF THE TENSILE STRENGTH OF GREEN CERAMIC SAMPLES FORMED BY DIFFERENT PROCESSING METHODS. THE WEIGHT PERCENT OF THE BINDERS IS SHOWN IN THE LEGEND. PVA IS POLYVINYL ALCOHOL, CARBOWAX IS A POLYETHYLENE GLYCOL, MAM IS METHACRYLAMIDE, PEG IS POYETHYLENEGLYCOL(1000)DIMETHACRYLATE, AND MBAM IS METHYLENEBISACRYLAMIDE.	14
FIGURE 7—TEST SAMPLES USED FOR RADIATION EXPOSURE TESTING AT KAERI AND OSURR.	16
FIGURE 8—TEST SAMPLES AFTER UNDERGOING 88.5 MRAD RADIATION EXPOSURE AT KAERI.....	16
FIGURE 9—COMPARISON OF THE FLEXURE STRENGTH OF ALUMINA SAMPLES BEFORE AND AFTER RADIATION EXPOSURE. FIVE SAMPLES WERE TESTED FOR EACH EXPOSURE LEVEL.....	18
FIGURE 10—COMPARISON OF THE THERMAL EXPANSION COEFFICIENT OF ALUMINA SAMPLES MEASURED BEFORE AND AFTER RADIATION EXPOSURE.	19
FIGURE 11—DILATOMETER PLOT SHOWING THE THERMAL EXPANSION OF ALUMINA SAMPLES BEFORE AND AFTER RADIATION EXPOSURE. FOR EACH EXPOSURE LEVEL THE LINE REPRESENTS THE AVERAGE VALUE OF SIX TESTS.....	19
FIGURE 12—OPTICAL MICROSCOPE IMAGES OF THE CROSS-SECTION OF THE LAMINATED ALUMINA SAMPLE SHOWING THE PT ELECTRODE AND THE INTERFACE REGION BETWEEN THE TWO ALUMINA LAYERS.....	20

Table of Tables

TABLE 1—SOME TYPICAL PROPERTIES OF THE CANDIDATE CERAMIC MATERIALS.	11
TABLE 2—WEIGHT CHANGE OF SAMPLES THAT UNDERWENT RADIATION EXPOSURE TESTING AT KAERI.	17

Table of Acronyms

EPRI-----	Electric Power Research Institute
KAERI-----	Korean Atomic Energy Research Institute
ID-----	Inside Diameter
LER-----	NRC Licensee Event Reporting database
NPP-----	Nuclear Power Plant
NRC-----	U.S. Nuclear Regulatory Commission
OD-----	Outside Diameter
ORNL-----	Oak Ridge National Laboratory
OSU-----	The Ohio State University
OSURR-----	The Ohio State University Research Reactor
SS-----	Stainless Steel

This Page Intentionally Left Blank

CERAMIC MATERIALS FOR PRIMARY LOOP MAGNETIC FLOWMETERS AT NUCLEAR POWER PLANTS

1 Project Summary

The primary objective of this project was to demonstrate the applicability of magnetic flowmeters to nuclear power plant (NPP) primary coolant flow measurement. Magnetic flowmeters (also referred to as electromagnetic flowmeters) are the most commonly¹ deployed industrial flowmeter type. Magnetic flowmeters are most applicable to situations requiring high accuracy measurement of high velocity liquid flows in large pipes—a situation that closely matches NPP primary flow. They have not previously been applied to NPPs because of the environmental sensitivity of currently available component materials. The technical focus of this project was on developing, fabricating, and then assessing the environmental survivability of the ruggedized components required to apply magnetic flowmeter technology to primary coolant loops of NPPs.

As the electronics required for a magnetic flowmeter can be remotely located from the piping, only the flowmeter sensing elements (referred to as the flowtube) need be significantly different for NPP applications as compared to other industrial applications. Water-applicable magnetic flowmeters require an electrically insulating pipe liner that isolates the measurement electrodes from each other as well as the pipe wall. Nuclear power plant primary coolant lines provide a harsh environment in terms of temperature, radiation, erosion, and chemical potential for the insulating pipe liner. Ceramic-liner type magnetic flowmeters can potentially endure all of the required conditions. Additionally, limited capability versions of this type of measurement system are already commercially available. However, ceramic-lined magnetic flowmeters are only available for pipe diameters less than 30 cm and currently cannot be employed for fluids with temperatures above 200 °C. Increasing the allowable piping diameter for ceramic-lined magnetic flowmeters by roughly a factor of three while increasing allowable operational temperatures up to 300 °C was the principal technical objective of this project.

Many combinations of ceramic materials and fabrication technologies were considered for the flowmeter. A two-layer, gelcast alumina ceramic liner with an embedded printed and fired-on platinum electrode structure was selected as the prototype structure for fabrication and subsequent environmental tolerance testing. The liner is intended to be heat-shrunk fit into standard stainless steel piping with electrical connection provided using commercially available, high pressure, electrical feedthrough connectors. The liner is designed to remain under compression throughout light water NPP temperature ranges. Samples of the flowmeter liner materials were fabricated and subjected to 1.8 MGy of gamma radiation – simulating fifteen years of exposure. No degradation of the irradiated samples was detected in subsequent testing for any of the relevant material properties. The test results confirm that the concept of a gelcast laminated alumina ceramic liner having an embedded electrode is a feasible approach for producing a large-scale, elevated-temperature, ceramic-lined magnetic flowmeter.

This project was a combined effort by Oak Ridge National Laboratory (ORNL), the Korean Atomic Energy Research Institute (KAERI), and The Ohio State University (OSU). ORNL had both the overall project management role as well as responsibility for

designing and fabricating the material samples while KAERI and OSU independently performed the materials irradiation and characterization.

2 Background

2.1 Project Rationale

Light-water cooled NPPs rely upon primary coolant flow measurements as part of total plant thermal power determination. As such, flow measurements are important from both safety and power production perspectives. Flowmeter uncertainty remains a significant concern to safe and efficient NPP operation. Federal regulations, 10CFR50 Appendix K, mandate an increment in the NPP thermal power safety margin equal to the amount of thermal power measurement uncertainty. Traditionally a measurement uncertainty of $\pm 2\%$ has been concluded to be adequate.² For a 1 GW_e plant, assuming a 5¢/kW-hr price and uninterrupted full power production, a 2% power decrement results in an \$8.8 million revenue loss per year. Further, if the coolant flow measurement is inaccurate, it becomes difficult to determine the root cause for electrical power output shifts, which may mask potential equipment deteriorations.

Several utilities have now received approval to reduce the measurement uncertainty margin based upon improved accuracy of reactor thermal power measurement. The reactor thermal power, neglecting for simplicity the small heat losses into the reactor cavity, steam generator, and support structures, can be determined from the product of the change in temperature of the coolant across the core and the coolant mass flowrate (on either the primary or secondary side of the steam generator). Due to the relative accuracy of mean coolant temperature measurement, most of the uncertainty in reactor thermal power measurement arises from uncertainty in the coolant mass flowrate. However, optimal (and perhaps not even acceptable) technology for implementing improved reactor flow measurement has yet to be developed. The NRC Licensee Event Report (LER) database indicates that both traditional (orifice and differential pressure; e.g. Venturi) and more advanced (ultrasonic; both cross-correlation and time-of-flight) flowmeters have resulted in repeated, significant thermal power measurement deviations with a particularly troubling increasing rate of reactor overpower events from ultrasonic flowmeters in recent years.

Significant recent³ and on-going⁴ efforts exist to improve currently deployed coolant flowmeter performance and to deploy improved flowmeter technology. NPP feedwater coolant flowmeter surveys and evaluations have previously been performed^{5,6} but have not included magnetic flowmeters—likely due to lack of compatibility with NPP environments of state-of-the-art magnetic flowmeter components. This project is directly focused on overcoming the material constraints that have previously prevented magnetic flowmeters from being considered for NPP deployment.

Uncertainty determination in NPP coolant flow measurement is non-trivial. Flow profiles tend to be hydrodynamically unstable with swirl velocities commonly reaching 5% (and occasionally exceeding 20%) of axial velocity.⁷ The long, straight pipe sections required for full development of flow profiles are generally unavailable for primary coolant flow measurement within containment. Also measurement system geometries are uncertain to a sufficient degree to impact the measurement accuracy. Both spatial and temporal

temperature variations compound the geometric uncertainties. Ultrasonic flowmeters are susceptible to imperfections in the pipe wall thickness, non-uniform thermal expansions, and lack of spatial correspondence of temperature and flow profiles. While Venturi flowmeters are sensitive to fouling in the throat region, the lack of fully developed flow profiles, and differential pressure tap line errors. Further, NPP primary flow profiles change with both operating conditions (e.g., pumping rate and valve position) and component wear. Finally, no flow test facilities are available to calibrate flowmeters at coolant flowrates (Reynolds numbers) found in operating NPPs, which necessitates extrapolating flowmeter calibration conditions to operating conditions.

Magnetic flowmeters have the potential for increased measurement accuracy for NPP coolant flow measurement as compared to either ultrasonic or constriction and differential pressure based flowmeters. Magnetic flowmeters are often selected industrially when the highest accuracy is required for high flow situations in large pipes. Magnetic flowmeters are particularly well suited to non-fully developed flow profiles such as primary coolant flow measurements as they respond to flows throughout the pipe as opposed to only those in relatively narrow ultrasonic beam paths. Additionally, the ceramic liner of a magnetic flowmeter distorts less with temperature requiring smaller temperature compensations in the measurement than competing technologies. Magnetic flowmeters are obstructionless. This means that they are less likely to foul and consume no pumping power. Moreover, being obstructionless, they produce less flow disturbance than wetted ultrasonic flowmeters.

Magnetic flowmeters, when properly implemented, are a highly reliable measurement technology. They are less vulnerable to leaks, particularly in welded-in form, than either wetted ultrasonic flowmeters or differential pressure based flowmeters. Magnetic flowmeters are also not vulnerable to any of the well-known performance and calibration difficulties of differential pressure tap lines and transmitters.

2.2 Magnetic Flowmeter Overview

2.2.1 Commercial Experience Base

Magnetic flowmeters are commonly deployed in the sanitary, chemical, pulp & paper, and food industries. Magnetic flowmeters remain the revenue leader in flowmeters⁸ and have now been commercially available for more than 50 years. More than 50 magnetic flowmeter manufacturers exist worldwide.⁹ Far more magnetic flowmeters are sold for liquid flow metering than any other modern-technology type of flowmeter. The most advantageous condition for deployment of a magnetic flowmeter is a situation requiring high accuracy measurement of a conductive fluid moving a high velocity in a large pipe.

2.2.2 Physical Principals of Operation

Magnetic flowmeters are based upon Faraday's Law of Magnetic Induction. One expression of Faraday's Law is that any conductor moving through a magnetic field will generate a voltage (V) across it proportional to the magnitude of the magnetic field (B) and its transverse velocity (v). M.K. Bevir in 1970 first modeled the anticipated magnetic flowmeter measured response as:¹⁰

$$V = \int v \cdot (B \times j) d\tau \quad (1)$$

where j is the Green's function describing the geometrical configuration of the electrodes that corresponds to the local current density arising from unit current passing between the opposing electrodes. The integration is performed over the entire volume of the liquid in the pipe.¹¹ For a measured voltage and a known magnetic field and system geometry a volumetric flowrate can be determined from Equation (1).

The conventional magnetic flowmeter sensor element essentially consists of a segment of non-magnetic pipe (stainless steel for NPP applications) that has been lined with an electrical insulator. A pair of electrodes penetrates opposite sides of the sensor body. Saddle shaped magnetic field coils are mounted outside the pipe and used to generate the internal magnetic field. Figure 1 provides a conceptual overview of a magnetic flowmeter. Conventional magnetic flowmeters have a pair of small electrodes that are in contact with the process fluid. First generation magnetic flowmeters had small electrodes and employed uniform magnetic fields. They were consequently oversensitive to flow near the electrodes.¹² Modern magnetic flowmeters with point electrodes employ shaped magnetic fields to minimize the flow profile sensitivity of the device. Alternatively, large area capacitively coupled electrodes can approximately integrate the voltage produced throughout the volume¹³ minimizing the measurement sensitivity to flow profile variation.

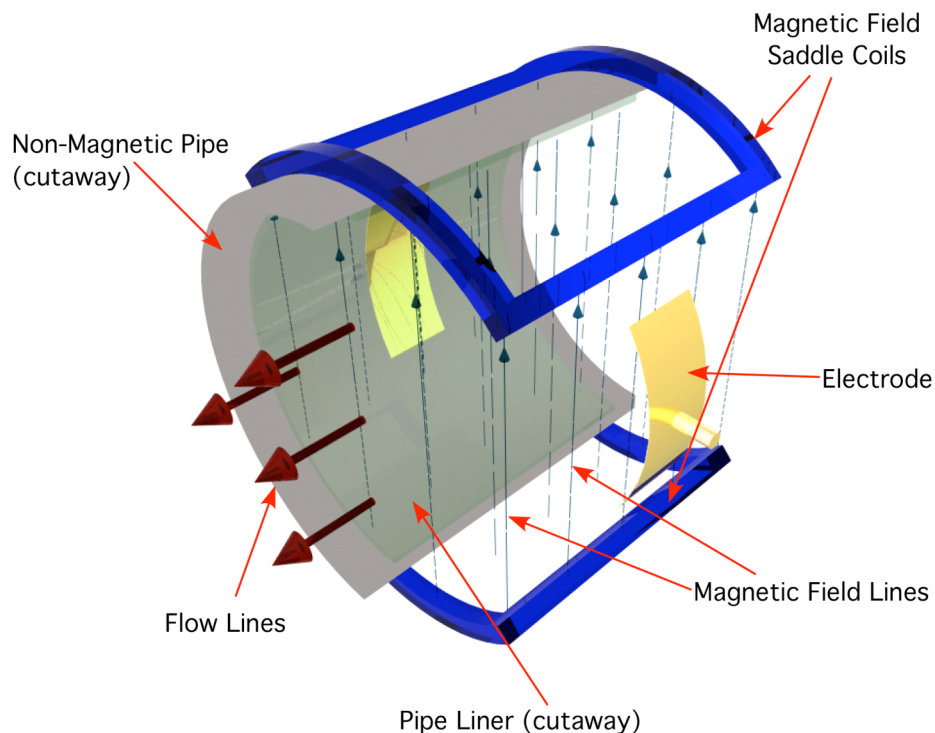


Figure 1—Conceptual illustration of a magnetic flowmeter with large size capacitively coupled electrodes

Magnetic flowmeter insulative linings are currently produced from most organic insulators and from glasses and ceramics (alumina and zirconia) for smaller (< 200 mm) pipe diameters. No currently available liner material can endure the required set of NPP environmental conditions.

Magnetic flowmeters are relatively small signal devices. The induced voltage at the electrodes is in the microvolt to millivolt range. Consequently, much of the recent magnetic flowmeter development work has gone into techniques to reject interferences and minimize measurement drift. Several different magnetic field excitation schemes have been developed. Both pulsed AC and dual frequency pulsed DC excitation are commonly used to maximize the system signal-to-noise ratio while minimizing the drift. Also, good grounding and shielding practices are required to transmit the signal to the measurement electronics. Magnetic flowmeter signals are also vulnerable to electromagnetic spikes and signal filtering is commonly required. Digital signal processing has also been implemented to reject non flow-related noise. Signal measurement electronics can generally be located several tens of meters away from the flowtube. As magnetic flowmeters are a fully commercial technology readily deployable to less harsh environmental conditions, this project restricted its focus to the materials aspects of magnetic flowmeters that have previously prevented their consideration for NPPs.

2.2.3 Advanced Architectures

While commercial magnetic flowmeters often have uncertainties as low as $\pm 0.25\%$ for larger velocity flows, NPPs exhibit particularly highly temporally and spatially varying flow profiles. Meter installation would also be considerably simplified if the minimum required three straight pipe diameters upstream and two downstream could be decreased. It may, therefore, be advantageous to deploy more advanced magnetic flowmeter architectures. Much as with the multi-path ultrasonic flowmeters, magnetic flowmeters can be deployed with multiple magnetic poles that are sequentially excited to provide a tomographic view of the flow profile.¹⁴ However, magnetic flowmeters are inherently more integrating than relatively narrow beam ultrasonic flowmeters. Employing shaped magnetic fields and large spatial extent electrodes further reduces the change in response to flow profile variations, so a multi-path deployment with its complications is of lesser importance than for an ultrasonic system. Finally, more advanced signal processing incorporating wavelet analysis for improved noise rejection and neural networks for system diagnostics may be useful for minimizing the measurement uncertainty.¹⁵

2.2.4 Operational Limitations

While a properly designed magnetic flowmeter based NPP primary coolant flow measurement system is anticipated to be highly accurate and reliable, magnetic flowmeters do have system limitations that need to be understood and addressed. Magnetic flowmeters are not a commodity product and models from different suppliers exhibit significant variance in accuracy under different flow conditions.¹⁶ Also magnetic flowmeters are almost never intended to function for multiphase flow or gas flow. This means that magnetic flowmeters would need to be employed on the feedwater lines of a boiling water reactor. Magnetic flowmeter signal strength increases linearly with flow velocity. At sufficiently low velocities, system accuracy is greatly reduced ($\pm 0.25\%$ at

> 2 m/s and \pm 5% at < 250 mm/s typical). Magnetic flowmeters also require replacing a pipe segment and as such are significantly more difficult and costly to deploy than clamp on ultrasonic flowmeters. Magnetic flowmeters are vulnerable to coatings accumulating on the electrically insulating liner, which both changes the effective volume of the flowmeter as well as the coupling to the electrodes. Also small voltage sources located roughly 30 m from first stage signal amplifiers are vulnerable to induced noise. Proper cable specification and deployment as well as grounding and shielding are critical to successful measurements. Finally, advanced magnetic flowmeter electrode and magnetic pole patterns are relatively complicated as compared to ultrasonic flowmeters and less progress has been made in incorporating advanced features into commercial magnetic flowmeters.

2.3 Competing Technologies

2.3.1 Venturi and Differential Pressure Based Flowmeter

Venturi meters and flow nozzles remain the most common technology for measuring coolant flow at NPPs. Both of these are essentially flow restriction and differential pressure based measurement systems. Both Venturis and flow nozzles are rugged devices with long service histories. However, they are vulnerable to fouling, require relatively longer straight pipe lengths, are subject to differential pressure tap line voids, blockages, and leakage, and in general exhibit lower overall long-term system accuracy as compared to their more modern alternatives. In addition, differential pressure measurements have accuracy under accident conditions as low as \pm 10%.¹⁷ The fouling problem with nozzle-based devices at NPPs is somewhat intractable as the pressure increase at the throat of the device induces condensation of required soluble chemicals. While progress has been made with noble metal coating the throats, the relatively lower reliability of differential pressure measurements limits the ability of these systems to improve their net uncertainty. Obstruction based flow elements also tend to be difficult to inspect and clean as they are within high-pressure piping. Moreover, obstruction based flowmeters always consume some pumping power as head loss across the flow measurement element. While the measurement errors due to throat fouling are conservative, they result in lost power production and can have as much as a 1-2% impact¹⁸

2.3.2 Ultrasonic Flowmeters

Ultrasonic flowmeters essentially consist of a set of transmitting/receiving ultrasonic transducers deployed across a pipe segment and associated signal processing software and hardware. Ultrasonic transducers may be deployed in wetted (pipe penetrating) or non-wetted (clamp-on) configurations although to date all NPP applications have involved wetted transducers. Both transit time and cross-correlation ultrasonic flowmeters have been used for NPP coolant flow measurement.

Transit time ultrasonic flowmeters function by sending and receiving pulses upstream and downstream from a pair of signal transducers (see Figure 2). The upstream moving pulses are retarded by the flow motion and take longer to reach the upstream-located transducer while the downstream moving pulses are accelerated by the liquid movement and reach the downstream transducer in a shorter time. The transit time of each of these

pulse streams is recorded, and from the combination of these two time measurements, the mean fluid velocity along the acoustic path can be determined. The accuracy of this measurement depends on the precision to which the pulse arrival time differences can be measured – nanosecond timing is required for precision measurement. This can be challenging in a NPP environment and timing related errors appear to be at the root of at least some of the recent overpower incidents. Figure 2 shows a single pair of ultrasonic transducers. The eight chord ultrasonic flowmeters that have been implemented at NPPs employ four pairs of transducers to correct for variances in the velocity profile. While this does decrease the number of straight pipe sections required, each transducer mount is another leak location vulnerability in the coolant loop. Transit time ultrasonic flowmeters both measure and correct for temperature variations in the coolant. One uncorrected source for uncertainty in the measurement is the assumption that the flow profile matches the temperature profile.

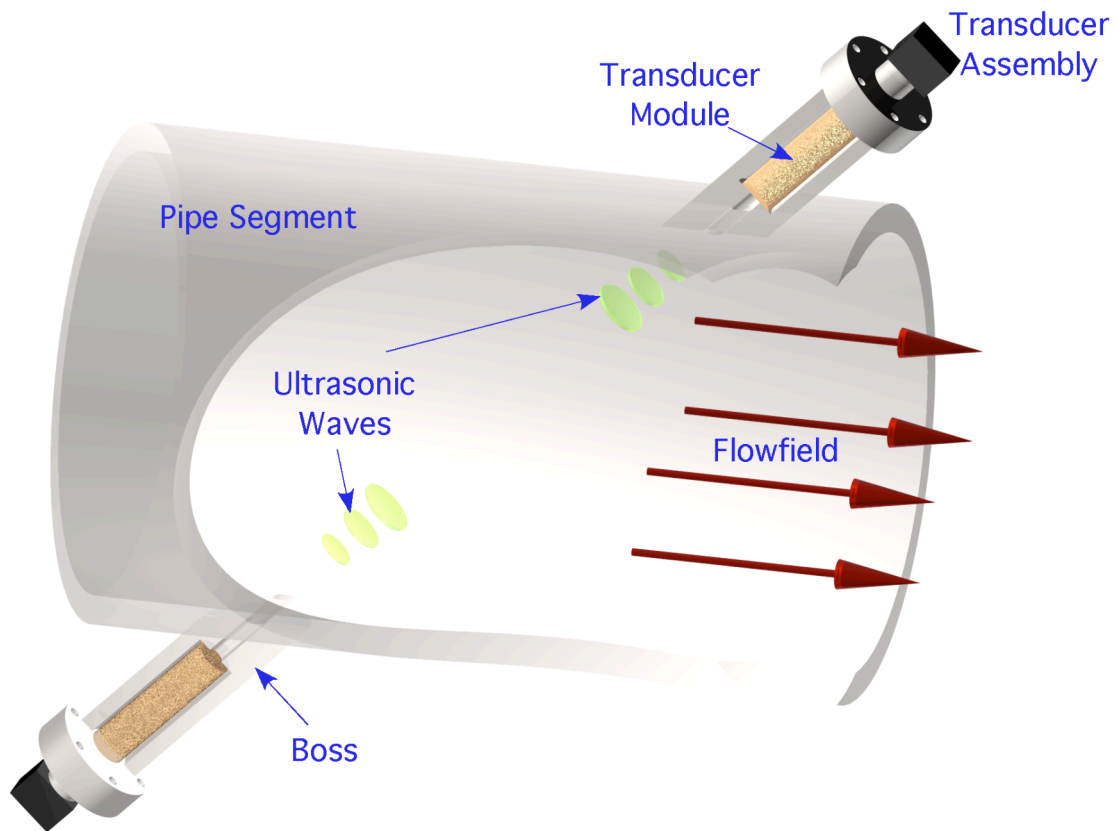


Figure 2—Transit Time Ultrasonic Flowmeter Conceptual Arrangement

Cross-correlation ultrasonic flowmeters make use of the time-delay between flow disturbances (e.g. eddies, swirl, or particulates) passing two ultrasonic beams—one located downstream of the other (see Figure 3). As the disturbances pass through the beams, the received signals will be altered in a correlated manner. Signal processing allows determination of the time-of-passage for the flow disturbances thereby providing a measure of mean flow velocity. Cross correlation flowmeters average many individual flow disturbances to obtain a mean flow velocity.

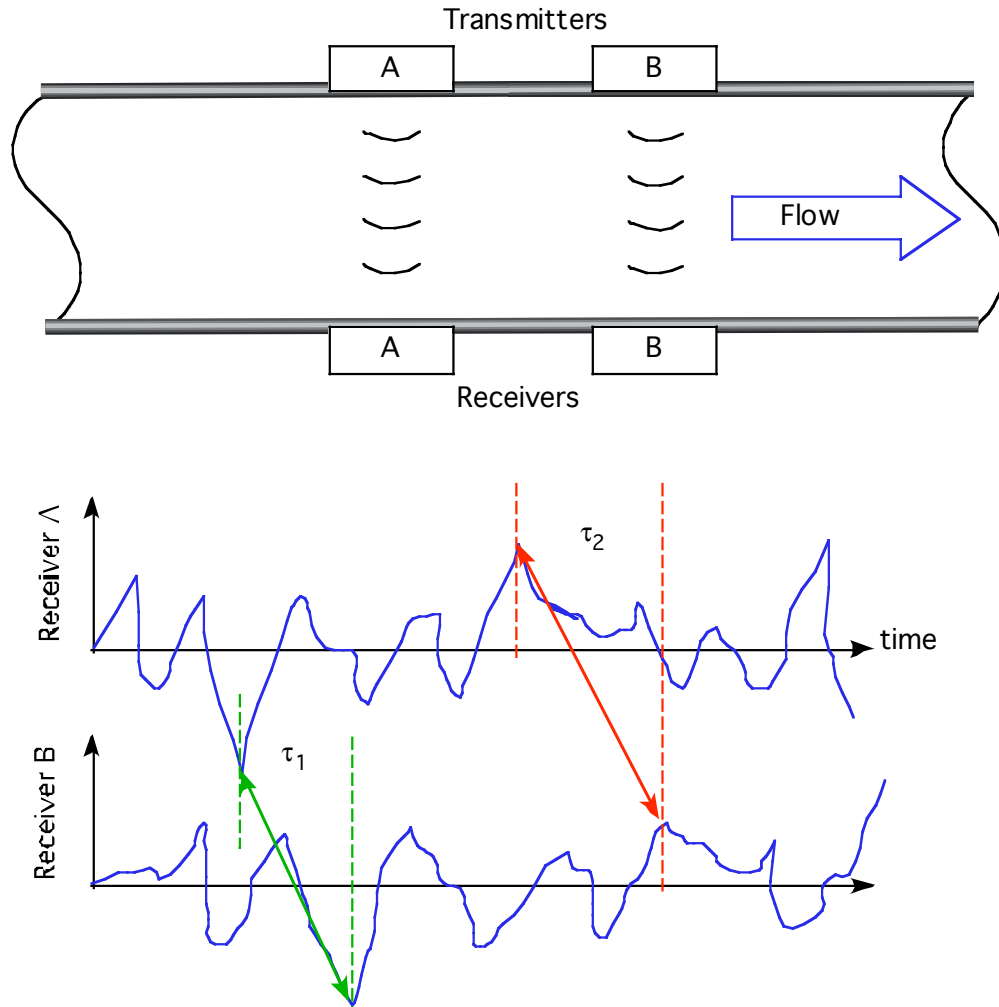


Figure 3—Conceptual Operation of Cross-Correlation Ultrasonic Flowmeter

Wetted ultrasonic flowmeters are much less sensitive to fouling than orifice based flowmeters. However, their uncertainties are not necessarily conservative and thus could potentially allow violation of plant operating technical specifications. While cross-correlation ultrasonic flowmeters are not subject to fouling, they are subject to imperfections in the pipe wall thickness and are more sensitive to non-uniform velocity profiles; all NPP applications to date employ a single cross-pipe measurement.

3 Experimental Approach

Temperature and radiation were judged to be the critical environmental variables that the ceramic flowtube must endure. As such, the experimental approach employed was to fabricate component samples, expose them to temperature and radiation and then measure their performance. Electrical continuity, thermal expansion coefficient change, mechanical strength, and component weight were the primary variables measured. Several characteristics of the ceramic must be considered for the flowmeter liner. Because of the pressurized condition in the pipe, the ceramic must have sufficient strength to resist fracture under normal operating conditions; therefore, adequate fracture strength is a critical factor. Since the ceramic liner will be contained inside a metal

housing, the closest possible match between the thermal expansion coefficients of the metal and ceramic is needed to avoid generating stresses in the materials during thermal cycling. The ceramic must be erosion and corrosion resistant under typical operating conditions, must have high electrical resistivity, and must be resistant to radiation damage. Consideration of the processing methods used to manufacture ceramic parts was of particular importance in identifying candidate materials and assessing feasibility.

To confirm that the materials to be used in the flowmeter assembly would be able to withstand the gamma radiation exposure expected during use, samples of all of the materials to be used in the flowmeter were prepared for exposure testing. Sets of sample materials were shipped to both KAERI and the OSU Research Reactor facility for radiation exposure. The samples were exposed to high-level gamma radiation from a ^{60}Co source. The total radiation dose was 1.8 MGy, which was calculated to be equivalent to 15 years of exposure under the normal radiation levels expected for the flowmeter in the service environment (13.5 Gy/hr) for primary coolant flow measurement applications. The high gamma exposure to the liner material arises from energetic neutron activation of Oxygen-16 ($^{16}\text{O}(n,p)^{16}\text{N}$) in the core. The half-life for Nitrogen-16 decay is only 7.13 s, so the cold-leg piping receives much less dose than the hot-leg piping. The exposures were performed over a 24-hour period. All of the test samples were weighed before and after exposure to determine whether the exposure would result in any change in mass.

The candidate ceramic material was machined into test bars measuring $4 \times 3 \times 45$ mm. The four-point flexural strength was measured on an Instron 4465 universal testing machine following the method described in the JIS R160:1995 testing standard. Results were compared for samples receiving 0, 0.9, and 1.8 MGy exposures. The flexural strength in four point bending was calculated by using the following equation:

$$S = \frac{3P(L-l)}{2wt^2} \quad (2)$$

where

- S = flexure strength,
- P = applied load at fracture,
- L = outer support span,
- l = inner span,
- w = specimen width, and
- t = specimen thickness.

The thermal expansion coefficient of the ceramic material was measured with a Setaram TMA92 dilatometer according to the ASTM E831 standard test method. A NIST standard reference material, 731 Borosilicate Glass, was used in the test. Three samples each of the ceramic materials irradiated with 0, 0.9, or 1.8 MGy were tested twice in the instrument. The test was performed in the temperature range of $25\text{ }^\circ\text{C} - 350\text{ }^\circ\text{C}$. The thermal expansion coefficients were calculated by using the following equation:

$$\alpha_m = \frac{1}{L_0} \frac{l(T_2) - l(T_1)}{T_2 - T_1} = \frac{1}{L_0} \frac{\Delta l}{\Delta T} \quad (3)$$

where

α_m = thermal expansion coefficient,

L_0 = specimen length at room temperature,

$l(T_1), l(T_2)$ = the specimen lengths at temperatures T_1 and T_2 ,

Δl = variation in specimen length between temperature T_1 and temperature T_2 ,

and

ΔT = temperature difference between T_1 and T_2 .

The proposed ceramic liner configuration consists of a 2-layer cylinder with the detecting electrode sandwiched between the layers. Coupon specimens of this configuration were fabricated for radiation exposure and property measurements. The coupons were approximately 50 x 50 mm and composed of two layers of bonded ceramic with a Pt electrode pattern located at the interface between the two layers. The inner and outer layer thicknesses were 3 mm and 5 mm, respectively. A screen printable Pt paste (Electro-Science Laboratories, Type 5547-IF-P) was used to apply an interconnected, but discontinuous electrode layer in the laminated structure. The discontinuous pattern allowed some direct contact areas between the two alumina layers, thus assuring a better bond at the interface. For preparing the test samples, a rubber stamp was used to apply the electrode pattern. The test sample form sent to KAERI and The Ohio State University Research Reactor (OSURR) is shown schematically in Figure 4. An important consideration in this design was whether the layered structure would remain bonded after the radiation exposure and whether the integrity of the embedded electrodes would be affected. After the radiation exposure was completed, the test samples were evaluated for degradation of the electrode and the layer interface bond.

The magnetic flowmeter requires an electrical connection between the detecting electrodes inside the stainless steel housing and the flowmeter electronics located external to the housing. A pressure-rated electrical feedthrough connector, Conax[®] TG-24-2¹⁹ was selected for this purpose. Each of the individual connector component materials, as well as fully assembled connectors, was subjected to radiation exposure. The connectors were subsequently tested for pressure seal integrity and electrical continuity.

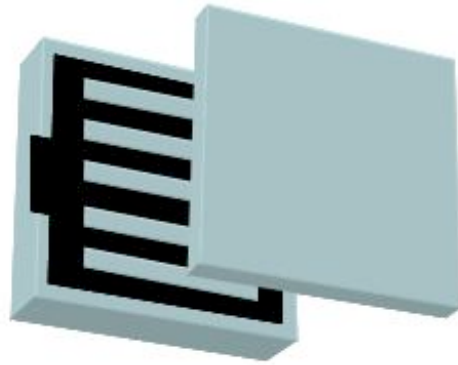


Figure 4— Illustration of the layered alumina ceramic test sample with an embedded Pt electrode used for radiation exposure testing at KAERI and OSURR.

4 Results and Discussion

4.1 Material, design, and process selection

Two candidate ceramic materials were identified that appear to have the needed properties for application to primary coolant flow measurement, alumina (Al_2O_3) and zirconia (ZrO_2). These ceramics can be formed by several different processing methods and can be sintered to full density. Both of these ceramics are high strength materials and have relatively high thermal expansion coefficients compared to other ceramics, which will lower the mismatch with the stainless steel housing ($\alpha = 17 \times 10^{-6}/^\circ\text{C}$ for Type 304 SS). They are also very hard, which makes them erosion resistant, and they are not affected by acidic or caustic solutions. In fact, alumina is commonly used as a container for high-temperature acids and bases.²⁰ No corrosion or erosion testing was performed for this project on fully-dense alumina as its known properties indicate that these stressors would not be limiting in NPP primary flow conditions. Relevant properties of these two ceramics are listed in Table 1.²¹ Alumina is one of the best-known electrical insulators and zirconia has good electrical resistance at low and moderate temperatures. The large size of the ceramic cylinder needed in the full-scale flowmeter will make the liner very difficult to fabricate. Alumina has a lower specific gravity than zirconia and thus would be a lighter weight part, which would be beneficial in all of the processing steps. Based primarily on its lower weight and excellent electrical resistivity, alumina was selected as the candidate ceramic material for subsequent property and performance evaluation.

Table 1—Some typical properties of the candidate ceramic materials.

Property	Units	Al_2O_3	ZrO_2
Density	g/cm^3	3.98	6.05
Flexure Strength	MPa	250 – 550	600 – 700
Compressive Strength	MPa	2500 - 3800	2000 - 2900
Modulus of Elasticity	GPa	380	205
Hardness	GPa	18 - 23	10 - 11
Thermal Expansion	$\times 10^{-6}/^\circ\text{C}$	7	9
Electrical Resistivity	ohm·cm	$> 10^{14}$	10^9

Initial assessment of the available technologies for manufacturing a large-scale, ceramic-lined magnetic flowmeter indicated that the approach which appeared to have the highest probability of success in this application was to cement a prefabricated ceramic cylinder with electrodes on the outer diameter surface into a stainless steel housing made of the same material as the coolant loop piping. The cement would act to bond the ceramic liner to the steel, electrically insulate the electrode from the housing, and create a transitional buffer (for properties such as thermal expansion coefficient) between the ceramic and the steel. However, upon further evaluation of the configuration it was determined that the close proximity of the electrode layer to the steel housing combined with a relatively thick dielectric layer (the alumina tube) separating the electrode from the fluid would result in a weak, degraded signal. A better design would be to reverse the relative thickness of the layers.

An alternative design would utilize a layered alumina cylinder having an embedded electrode layer near the inside diameter surface. This cylinder could be shrink-fitted into the stainless steel housing. The shrink fitting procedure would produce a compressive force on the cylinder and would eliminate the need for a cement to hold the ceramic liner in place. To estimate the stresses on the components and the temperature needed for the shrink-fitting process, a hypothetical magnetic flowmeter was selected for evaluation. The example consisted of an alumina liner having an inside diameter (ID) of 787 mm (31 in) and an outside diameter (OD) of 813 mm (32 in). Type 304 stainless steel was selected as the material for the metal housing. Based on the thermal expansion coefficient, α , at 300 °C the OD of the ceramic liner would expand to 814 mm (32.0616 in.). As a maximum, the ID of the housing should be the same as the OD of the liner at 300 °C. Using α for 304 SS to calculate the shrinkage on cooling, this corresponds to an unstrained (stress free) ID of 811 mm (31.9117 in.) at 25 °C. The ceramic liner could be inserted by heating the steel housing to 350-400 °C. With the liner in place, the housing would be constrained from shrinking fully upon cooling to room temperature, resulting in a tensile stress in the steel and a compressive stress in the ceramic. To estimate the stress level, the standard mechanical relationship, $\sigma = \epsilon E$, was used where σ is the stress, ϵ is the strain, and E is the elastic modulus (193 GPa for 304 SS and 380 GPa for alumina). A series of iterative calculations were made to balance the tensile stress and strain in the steel housing with the compressive stress and strain in the ceramic liner. The equilibrium stress level at 25 °C was estimated to be 354 MPa. This value is much lower than the compressive strength of the ceramic (2500-3800 MPa). However, because of the brittle nature of the alumina, it will be critical to insure that the mating surfaces of the housing and the liner are perfectly cylindrical so that the stresses will be applied uniformly around the circumference of the liner material.

Fabrication of the layered ceramic liner could be accomplished by using a two-step gelcasting procedure. Gelcasting is a ceramic forming process that was developed as a simple and economical method for producing large and/or complex-shaped advanced ceramic components.²²⁻²⁷ Gelcasting was developed by combining traditional ceramic slip processing with polymer chemistry. A flow diagram detailing the processing steps is shown in Figure 5. In the gelcasting process, a concentrated slurry of ceramic powder in a solution of organic monomers is poured into a mold and then polymerized *in situ* to

form a green body in the shape of the mold cavity. The monomer solution provides a low-viscosity vehicle to transport the fluid slurry into the mold and the polymer gel holds the ceramic powder in the desired shape. The result is a very homogeneous cast body, which shows a uniform chemical and density cross-section. Consequently, shrinkage during drying and firing is uniform (minimizing distortion) and material properties are constant throughout the body. Vinyl monomers are used in the process and, because they undergo a free-radical chain polymerization reaction, the setting is very rapid. Chain-forming monomers that are frequently used for water-based gelcasting include Methacrylamide and N-(Hydroxymethyl)acrylamide. Cross-linking monomers, which connect the polymer chains to form the gel network, include N, N'-Methylenebisacrylamide and Polyethyleneglycol(1000)dimethacrylate. The polymerization reaction is initiated with a free-radical source, such as Ammonium persulfate. The catalyst N,N,N',N'-Tetramethylethylenediamine may be used to accelerate the reaction.

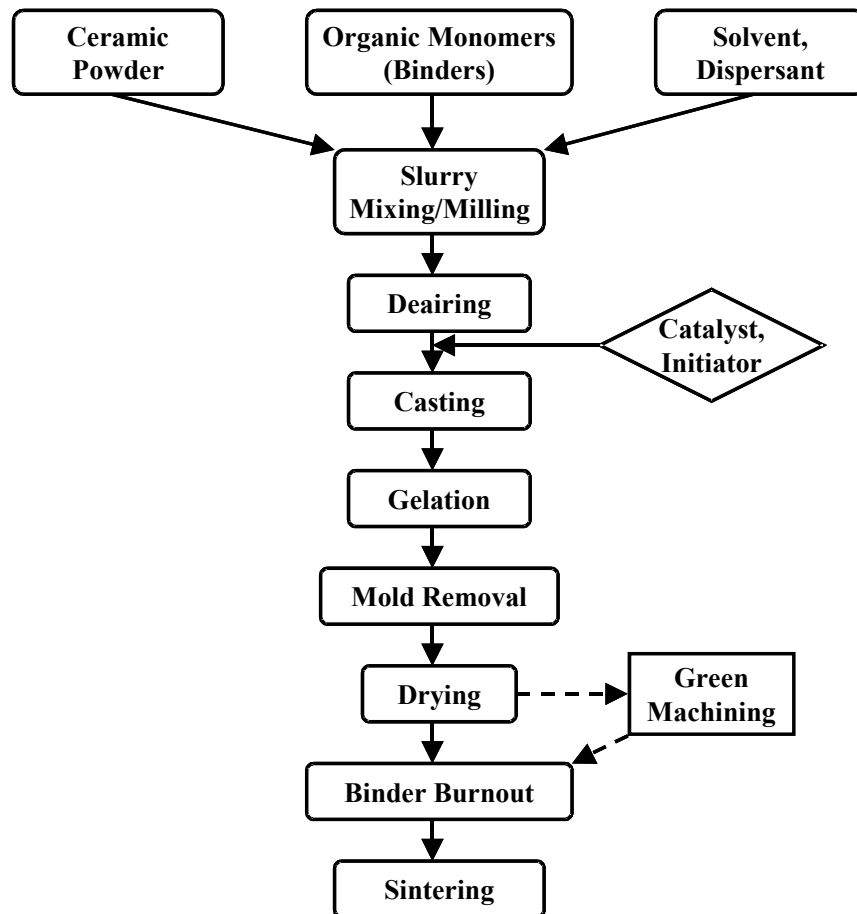


Figure 5— Flowchart showing the sequence of operations in the gelcasting process.

A wide range of ceramic powders, including alumina, has been processed using the gelcasting system. The slurry base is usually water, although non-aqueous solvents can also be used. The powder and monomers are combined in the solvent base along with a dispersant. The dispersing aid interacts electrochemically with the powder particles to prevent flocculation and settling. This allows the slurry to contain a high volume fraction

of powder (typically 50 vol.% or more) while retaining a low viscosity so that it can be easily poured into the mold. A high solids content is desirable to minimize shrinkage during drying and to promote densification during the sintering step.

The mixing and milling operation is accomplished with standard ceramic processing equipment, such as a ball mill or attritor mill. Once the mixing operation is complete, the slurry is de-aired under vacuum to remove entrained gas. The catalyst and initiator are then added prior to casting. Casting mold materials that have been used successfully for gelcasting include metal, plastic, wax, and glass. Each material must be tested for compatibility with the gelcasting chemicals.

Gelation can be accomplished under a broad range of conditions depending primarily on the amount of catalyst and initiator added to the slurry. Gelling can occur at temperatures ranging from ambient to 85 °C and go to completion in from 5 min. to 1 hr. Once gelled, the slurry forms a rigid body that can be removed from the mold. The cast part is then dried to remove the water that is trapped within the gel structure. Linear shrinkage of 2-3% can be expected during drying as the gel collapses until the ceramic powder particles come into contact and form a rigid network. For thick and/or large parts, the drying step must be carefully controlled to prevent uneven shrinkage that can result in distortion or cracking.

After drying is complete, gelcast ceramics form very strong green (unfired) bodies. A study to examine the strength of green ceramics formed by different processing methods found that gelcast parts could be more than 10 times stronger than parts formed by conventional ceramic forming methods.²⁸ The results of the study are shown graphically in the chart in Figure 6. High strength in the green body is particularly important for handling large, heavy parts, which could otherwise be easily damaged. Gelcast parts may be machined after drying.²⁹ This can be useful for producing prototypes or to form features that would add too much complexity to the mold.

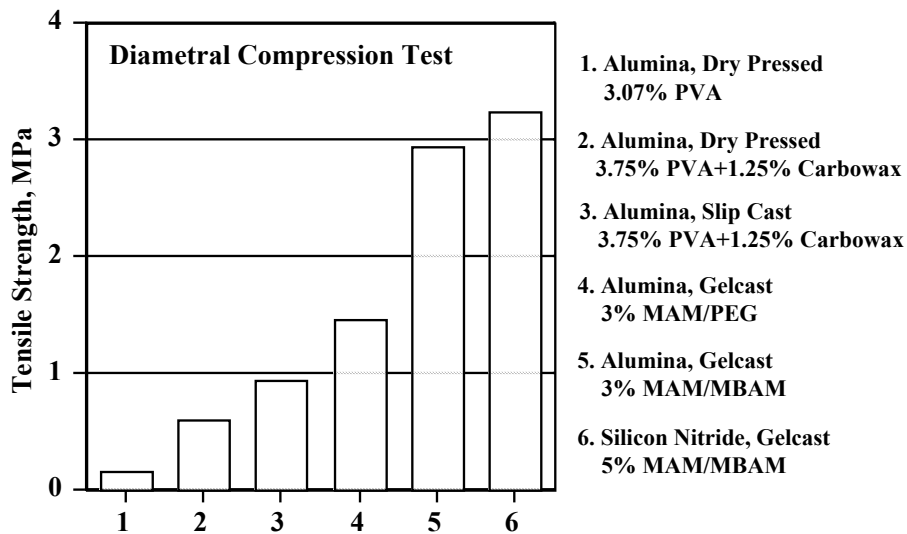


Figure 6—Comparison of the tensile strength of green ceramic samples formed by different processing methods.²⁸

The weight percent of the binders is shown in the legend. PVA is polyvinyl alcohol, Carbowax is a polyethylene glycol, MAM is methacrylamide, PEG is polyethyleneglycol(1000)dimethacrylate, and MBAM is methylenebisacrylamide.

The final processing steps for gelcast ceramics are the same as for conventionally formed ceramic parts. The organic binders, in this case the polymerized monomers, are removed from the part by pyrolysis. This is accomplished by heating the part to a temperature greater than 400 °C. High temperature sintering can be a continuation of the binder burnout step or a separate operation. For alumina, sintering takes place at about 1500 °C. At this temperature, diffusion processes act to consolidate the ceramic into a fully dense material.

In the first step of fabricating a layered ceramic flowmeter liner, a thin-walled ceramic cylinder would be gelcast and Pt electrodes applied by screen printing to the outside surface. A second, thicker cylinder would then be gelcast against the electroded surface of the first casting, resulting in an embedded electrode. The sintering process that is used to densify the alumina ceramic would hermetically seal the electrode inside the cylinder wall.

A commercial ceramic manufacturer with experience in gelcasting large plate and cylinder components was identifiedⁱ and would be a potential supplier of the large-scale laminated ceramic liners proposed for the production of magnetic flowmeters.

4.2 Radiation exposure and property evaluation

Samples of all of the materials for radiation testing are shown in Figure 7. These include: alumina tiles, 304 SS coupons, gelcast alumina with an embedded Pt electrode, assembled Conax[®] high-pressure electrical feedthrough connectors, Conax[®] lava sealing material, and Conax[®] electrical insulators. Sets of the test samples were sent to KAERI and OSURR for radiation exposure. The sample appearance after an exposure of 0.85 MGy in the KAERI radiation facility is shown in Figure 8. A slight change in the color of some of the samples was noted, otherwise, no significant changes were observed.

ⁱ Kikusui Chemical Industries Company of Japan, represented in the U.S. by Marketech International, Inc. see <http://www.mkt-intl.com/ceramics/ReptonBrochure.pdf>

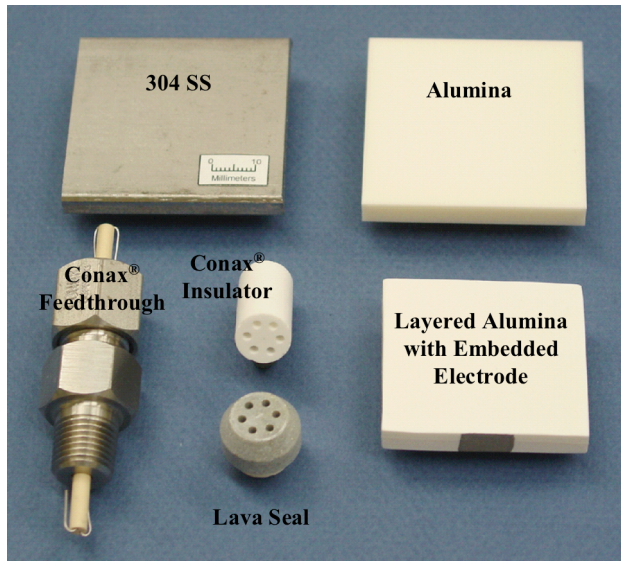


Figure 7—Test samples used for radiation exposure testing at KAERI and OSURR.

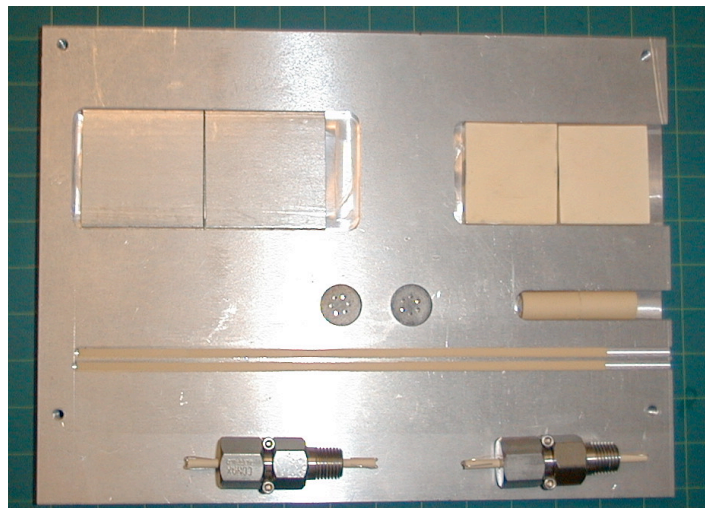


Figure 8—Test samples after undergoing 88.5 Mrad radiation exposure at KAERI.

Table 2—Weight change of samples that underwent radiation exposure testing at KAERI.

Sample		Weight, g		
		Before Irradiation	After Irradiation	
			885 kGy	1.77 MGy
Layered Alumina with Internal Electrodes	1	52.534	52.534	52.534
	2	51.026	51.026	51.026
Conax TG-24-2 Electrical Feedthrough	1	85.314	85.314	85.315
	2	85.099	85.099	85.101
Conax Lava Pressure Sealant	1	5.0128	5.0131	5.0155
	2	4.9745	4.9751	4.9792
Conax Electrical Insulator	1	9.5491	9.5491	9.5493
	2	9.5927	9.5927	9.5929
Type 304 Stainless Steel	1	127.348	127.348	127.348
	2	127.884	127.883	127.883
Alumina Bars (4 x 3 x 45 mm)	1	2.0609	2.0610	2.0610
	2	2.0627	2.0627	2.0627
	3	2.0686	2.0686	2.0645
	4	2.0539	2.0540	2.0371
	5	2.0558	2.0558	2.0560
	6	2.0655	2.0655	N/A
	7	2.0670	2.0670	N/A
	8	2.0652	2.0652	N/A
	9	2.0652	2.0652	N/A
	10	2.0631	2.0632	N/A

Evaluation of the samples after completion of the radiation exposure showed no significant changes in the dimensions or weights of the samples. As seen in Table 2, for the samples tested at KAERI, the weight changes were negligibly small with the largest measured change being less than 0.1% for the Conax[®] lava pressure sealant material.

The flexure strength of the alumina ceramic was compared for samples before and after radiation exposure. Five samples were tested for each radiation exposure level: 0, 0.85, and 1.8 MGy. The strength tests were performed at KAERI, and the results are shown in Figure 9. The flexure strength test measurements show that there was no degradation of the material strength after exposure to gamma radiation that was the equivalent of 15 years service in the reactor environment. There actually appears to be a slight increase in strength, although this may not be significant since the error bars for all of the sample sets overlap.

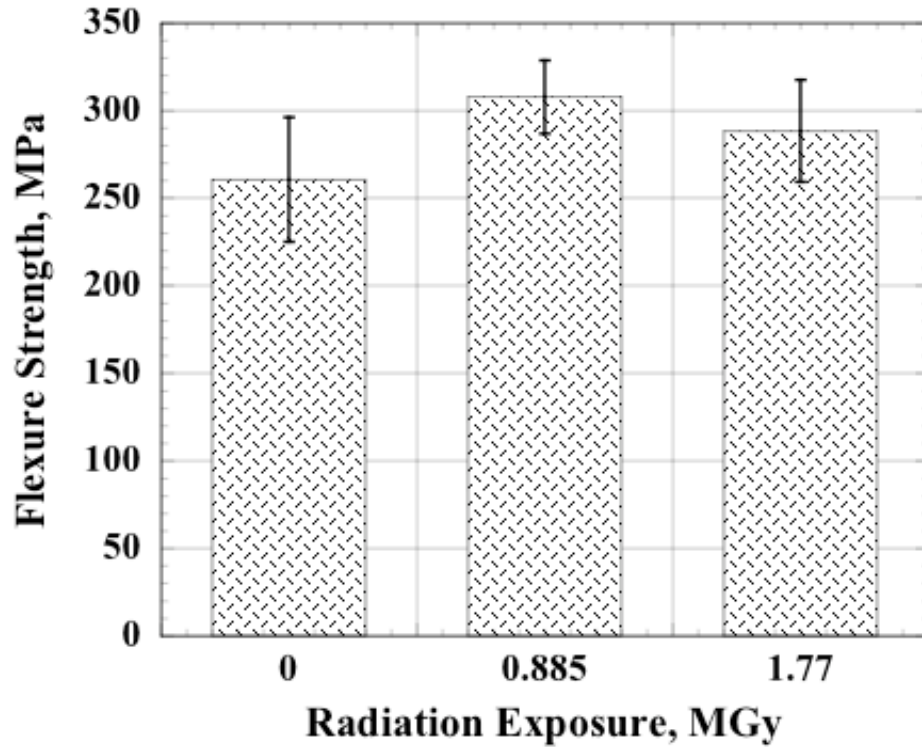


Figure 9—Comparison of the flexure strength of alumina samples before and after radiation exposure. Five samples were tested for each exposure level.

The results of the thermal expansion coefficient (α) measurements conducted at KAERI are shown as Figure 10. There was no discernable change in α for the three different levels radiation exposure. When the dilatometer data was averaged for all of the samples in each group and plotted simultaneously (Figure 11), the traces were virtually overlapping.

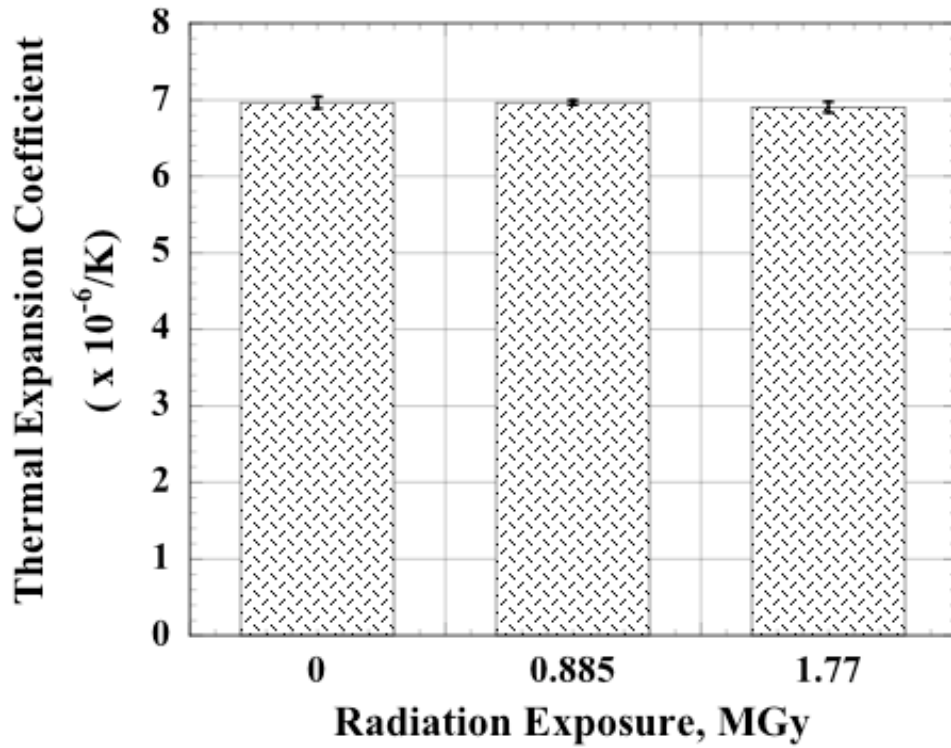


Figure 10—Comparison of the thermal expansion coefficient of alumina samples measured before and after radiation exposure.

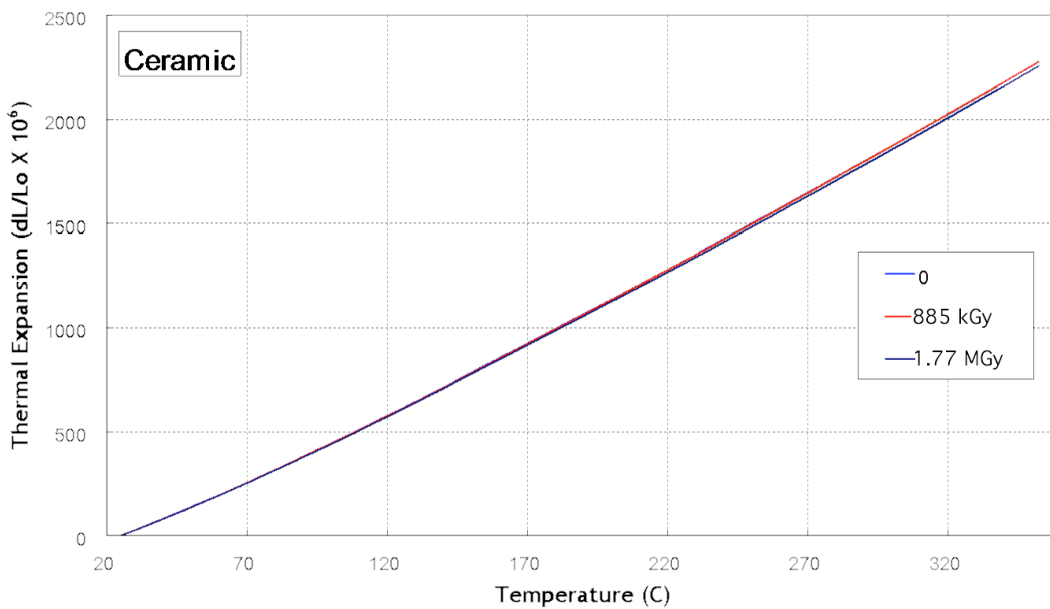


Figure 11—Dilatometer plot showing the thermal expansion of alumina samples before and after radiation exposure. For each exposure level the line represents the average value of six tests.

4.3 Component assembly evaluation

Of particular interest in the exposure tests was the determination of any effects on the laminated alumina material and the Conax[®] high-pressure electrical feedthrough. The electrical continuity of the Pt electrode embedded in the laminated alumina material was checked with a volt-ohm meter. A good electrical connection was observed between external contact points on opposite edges of the samples measured at OSURR and ORNL. One of the laminated specimens that had undergone irradiation exposure was cross-sectioned at ORNL to examine the internal electrode layer and the interface where the two alumina layers were joined. Optical micrographs of the sample cross-section are shown in Figure 12. The measured thickness of the Pt electrode seen in the micrographs is between 5 and 10 microns. Examination of the electrode and the interface region shows no indication of degradation of the irradiated material. The images show no structural difference between the alumina in the interface region and in the bulk of the material. There is no evidence of any damage to the interface bond due to the radiation exposure.

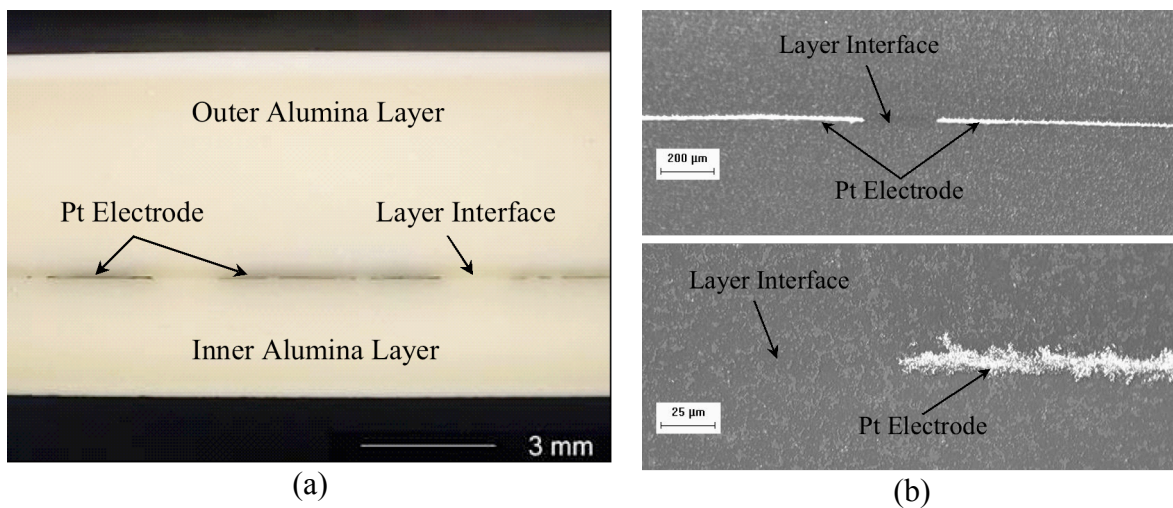


Figure 12—Optical microscope images of the cross-section of the laminated alumina sample showing the Pt electrode and the interface region between the two alumina layers.

The Conax[®] high-pressure electrical feedthrough is made up of several different materials, comprising the housing, insulators, and seal. The assembly was subjected to irradiation to assure that both electrical continuity and the pressure seal would be maintained after exposure. No significant changes were observed in the sealing material and the electrical insulating material that were exposed outside the assembly. Tests of the assembled feedthroughs after exposure showed good electrical continuity with no shorting to the feedthrough body. The irradiated assemblies were checked for pressure seal integrity at ORNL and OSURR and no detectable helium leaks were found at 15 MPa (2200 psi).

5 Conclusions

The primary objective of this project was to demonstrate the applicability of magnetic flowmeters to NPP primary coolant flow measurement. Magnetic flowmeters have not previously been applied to NPPs because of the environmental sensitivity of currently available liner materials and the general unavailability of large scale ceramic liners. The technical focus of this project was on developing, fabricating, and then assessing the environmental survivability of the ruggedized ceramic liner, electrodes, and electrical feedthrough required to apply magnetic flowmeter technology to primary coolant loops of NPPs. The in-containment locations for primary coolant piping provide a severe environment for the flowmeter liner materials. In a pressurized water reactor, the water is at 15 MPa (2200 psi) and about 300 °C, and chemical additions to the water maintain the pH at a mildly caustic level of 9.4. In addition, the interior liner materials for primary coolant loops are continually subjected to a high gamma radiation dose due to the activation of Oxygen-16 in the coolant water. Many ceramic materials were considered for the liner by examining the available property data. Alumina was selected as the candidate ceramic material for subsequent property and performance evaluation.

A proposed design was developed for the flowmeter liner that would utilize a layered alumina cylinder having an embedded electrode near the inside diameter surface. This cylinder would be then shrink-fitted into a stainless steel flowmeter housing. The shrink fitting procedure would produce a compressive force on the cylinder and would eliminate the need for a cement to hold the ceramic liner in place. Fabrication of the ceramic cylinder liner could be accomplished by using a two-step gelcasting procedure.

Samples of the flowmeter materials were prepared for irradiation testing to confirm that they would be able to withstand the gamma radiation exposure expected during use. The samples were exposed to a total gamma radiation dose of 1.8 MGy, which was calculated to be equivalent to 15 years of exposure in the hot-leg environment (note the cold leg environment would have much lower gamma dose as Nitrogen-16 only has a 7.13 s half-life). No degradation of the materials was detected in property evaluation tests conducted after the exposure.

The test results confirm that the concept of a gelcast laminated alumina ceramic liner having an embedded electrode is a feasible approach to producing a large-scale, ceramic-lined magnetic flowmeter. A commercial ceramic manufacturer with experience in gelcasting large components has been identified and would be a likely candidate to supply the laminated ceramic liners for the production of large-scale flowmeters.

¹ Jesse Yoder, *Trends Among the Top 10 Flowmeter Technologies*, Control Magazine, July 2003

² NRC Regulatory Guide 1.49, "Power Levels of Nuclear Power Plants"

³ EPRI TR-1004582, *Measuring Feedwater Flow With Ultrasonic Flow Meters*, December 2001

⁴ EPRI Project S68.008 "Demonstration of Clamp-on Ultrasonic Flowmeters for Feedwater Flow Measurement", project description available at <http://www.epri.com>

5 H.M. Hashemian, E.T. Riggsbee, D.W. Mitchell, M. Hashemian, C.D. Sexton, D.D.
Beverly, and G.W. Morton, *Advanced Instrumentation and Maintenance Technologies
for Nuclear Power Plants*, NUGREG/CR-5501, August 1998

6 EPRI TR-101388, *Feedwater Flow Measurement in U.S. Nuclear Power Generation
Stations*, November 1992

7 E. Hauser, J. Regan, and H. Estrada, *Impact of Flow Velocity Profile on Ultrasonic
Measurement Accuracy For Feedwater Flow in Nuclear Power Plants*, Proceedings of
ICONE10, 10th International Conference on Nuclear Engineering, Arlington, VA, April
14-18, 2002, pp. 1-7

8 <http://flowresearch.com/Worldmagneticflow-Rev-2.htm>

9 David W Spitzer and Walt Boyes, *The Consumer Guide to Magnetic Flowmeters, Second
Edition*, Copperhill and Pointer, Inc.; (August, 2003)

10 M.K. Bevir, *The theory of induced voltage electromagnetic flowmeters*, Journal of Fluid
Mechanics, **43**(3), 16 Sept. 1970, pp. 577-90

11 J. Hemp and H.K. Versteeg, *Prediction of electromagnetic flowmeter characteristics*,
Journal of Physics D: Applied Physics, **19** (1986), pp. 1459-1476

12 J. Hemp, *Improved magnetic filed for and electromagnetic flowmeter with point
electrodes*, Journal of Physics D: Applied Physics, **8**, 1975, pp. 983-1002

13 T.J. Cox and D.G. Wyatt, *An electromagnetic flowmeter with insulated electrodes of
large surface area*, Journal of Physics E: Scientific Instruments, **17**, 1984, pp 488-503

14 Taiichi Teshima, Satoshi Honda, and Yutaka Tomita, *Electromagnetic Flowmeter with
Multiple Poles and Electrodes*, Proceeding of Instrumentation and Measurement
Technology Conference, 1994. IMTC/94, **3**, 10-12 May 1994, Hamamatsu, Japan, pp.
1221-1224

15 R. Gao, E. Eryurek, and L. H. Tsoukalas, *A Novel Neural-Wavelet Diagnostics
Approach: Application to Magnetic Flowmeter*, International Journal on Artificial
Intelligence Tools, **10**(3), (2001), pp. 421-429

16 http://www.flowmeterdirectory.com/flowmeter_artc/flowmeter_artc_03112701.html

17 J. Weiss, W. Esselman, and R. Lee, *Assess fiberoptic sensors for key powerplant
measurements*, Power, October 1990: pp. 55-58

18 EPRI TR-1004582, *Measuring Feedwater Flow With Ultrasonic Flow Meters*, December
2001

19 http://www.conaxbuffalo.com/products/pres_vac.html

20 J.R. Blachere and F.S. Pettit, High Temperature Corrosion of Ceramics, William Andrew
Publishing/Noyes, 1989

21 Engineered Materials Handbook, Vol. 4, Ceramics and Glasses, ASM International,
1991.

22 M. A. Janney and O. O. Omatete, *Method for Molding Ceramic Powders Using a Water-
Based Gelcasting*, U. S. Pat. No. 5 028 362, July 2, 1991.

23 A. C. Young, O. O. Omatete, M. A. Janney, and P. A. Menchhofer, *Gelcasting of
Alumina*, Journal of the American Ceramic Society, **74** [3] (1991), pp. 612-618.

24 O. O. Omatete, M. A. Janney, and R. A. Strehlow, *Gelcasting—A New Ceramic Forming
Process*, American Ceramic Society Bulletin, **70** [10] (1991), pp. 1641-1649.

25 M. A. Janney and O. O. Omatete, *Method for Molding Ceramic Powders Using a Water-
Based Gelcasting Process*, U. S. Pat. No. 5 145 908, Sep. 8, 1992.

26 Ogbemi O. Omatete, Mark A. Janney, and Stephen D. Nunn, *Gelcasting: from
Laboratory Development Toward Industrial Production*, Journal of the European
Ceramic Society, **17** (1997), pp. 407-413.

-
- ²⁷ M. A. Janney, O. O. Omatete, C. A. Walls, S. D. Nunn, R. J. Ogle, and G. Westmoreland, *Development of Low-Toxicity Gelcasting Systems*, Journal of the American Ceramic Society, **81** [3] (1998), pp. 581-591.
- ²⁸ S. D. Nunn, O. O. Omatete, C. A. Walls, and D. L. Barker, *Tensile Strength of Dried Gelcast Green Bodies*, Ceramic Engineering and Science Proceedings, **15** [4] (1994), pp. 493-498.
- ²⁹ S. D. Nunn and G. H. Kirby, "Green Machining of Gelcast Ceramic Materials," Ceramic Engineering and Science Proceedings, **17** [3] (1996), pp. 209-213.